Comparison between vibration and stator current analysis for the detection of bearing faults in asynchronous drives

Baptiste Trajin, Jérémi Regnier, Jean Faucher

Comparison between vibration and stator current analysis for the detection of bearing faults in asynchronous drives

B. Trajin[1,2] *J. Regnier*[1,2] *J. Faucher*[1,2]

[1]*LAPLACE (Laboratoire Plasma et Conversion d'Energie), Université de Toulouse; INP, UPS; ENSEEIHT, 2 rue Camichel, BP7122, F-31071 Toulouse Cedex 7, France*
[2]*CNRS; LAPLACE; F-31071 Toulouse, France*
E-mail: baptiste.trajin@laplace.univ-tlse.fr

Abstract: This study deals with the application of vibration and motor current spectral analysis for the monitoring of rolling bearings damage in asynchronous drives. Vibration measurement is widely used to detect faulty bearings operations. However, this approach is expensive and cannot always be performed, while electrical quantities such as the machine stator current are often already measured for control and detection purposes. Signal processing methods and global indicators associated with bearing fault detection of vibration measurements are recalled. Compared to these methods, an automatic detector based on vibration spectral energy extraction is then proposed and its performances are discussed. Moreover, load torque measurements underlines that bearing faults also induce mechanical load torque oscillations. Therefore a theoretical stator current model in case of load torque oscillations is used to demonstrate the presence of phase modulation (PM) on stator currents. Frequency behaviour of the related sideband components is strongly investigated for monitoring purposes. Thus, a fault detector using the extraction of spectral energy of stator current is proposed to detect damaged bearings. This detector is then compared to the one defined on vibration signals.

1 Introduction

Electrical drives using induction motors are widely used in many industrial applications because of their low cost and high robustness. However, many types of faulty operations could appear during the lifetime of the system. A large overview of electrical machines failures and monitoring technics can be found in [1]. A classification of the most frequently encountered faults can be found in [2]. To improve the availability and reliability of the drive, a condition monitoring could be implemented to favour the predictive maintenance. Traditionally, motor condition is supervised using vibration analysis [3] but measuring such mechanical quantities is often expensive. Indeed vibration sensors such as piezoelectric accelerometers and associated load amplifier are often expensive. Moreover, the ability of a clear detection of bearing faults by vibration measurements lies in the sensor locations. Indeed, accelerometers need to be mounted near to each possible faulty bearing of the machine.

To overcome this problem, the detection could be based on the measurement of stator currents which are often available for control purposes. A general review of monitoring and fault diagnosis schemes using stator current is available in [4]. As shown in [2], the major faults come from faulty bearings. In this case, several studies demonstrate that specific signatures appear on stator current spectrum [5]. A comparison between vibration and stator current monitoring has been presented in [6]. A model for bearing fault detection has been proposed in [5, 7], based on the assumption that bearing defects lead to a particular airgap eccentricity and thus induce the characteristic signatures on stator current spectrum. Other studies consider that bearing faults induce load torque oscillations [8]. Then, spectral techniques are often applied to detect and classify such phenomena. Therefore the definition

of an indicator performing an automatic extraction of relevant information from the current spectrum is rarely of concern [9]. This work presents the design and validation of a novel automatic indicator for bearing faults detection based on energy extraction from stator current spectrum. The efficiency of such a detector is compared to a similar mechanical automatic detector based on vibration analysis.

In this paper, an overview of methods for the detection and diagnosis of defects in ball bearings is firstly recalled in Section 2. A basic automatic detector based on vibration spectral energy extraction is proposed to detect bearing faults with a good confidence rate and its performances are compared with other methods. Section 3 studies the effects of bearing faults on mechanical quantities such as eccentricity and load torque. It is demonstrated that airgap variation and thus eccentricity induced by bearing defects may be considered as negligible. Consequently, the paper focuses on load torque variations due to bearings faults. In Section 4, a stator current model that demonstrates that sideband components due to load torque oscillations exist in the current spectrum is recalled. A gain diagram is established to study the amplitude of these specific sidebands related to the load torque oscillation frequency. In Section 5, an automatic detection based on current spectral energy estimation is proposed to detect faulty bearings. Restrictions of the proposed indicator regarding its definition and the use of the gain diagram are then discussed as well as a general comparison between vibration and stator current detectors. Finally, some suggestions are proposed to choose a detection method regarding to the system that has to be monitored.

2 Vibration analysis for bearing faults

In this paper, three different types of bearings are studied. Bearings are mounted in a 5.5 kW, two pole-pairs induction machine supplied by a variable frequency inverter. An acquisition board is used to sample vibrations, load torque and stator currents. First of all, two 6208-type bearings are modified using electro-erosion to create a 3 mm-large hole in the full width of the outer or inner raceway. A photograph of an inner race artificial fault is given in Fig. 1. These single point defects are comparable to the worst case of the effect of spalling due to a severe ineffective lubrication [10]. The third bearing is a healthy one used as a reference.

2.1 Characteristic bearing fault frequencies

Faulty bearings characteristic frequencies are theoretically well known. Moreover, frequency harmonics due to defects could appear as combinations of characteristic frequencies, cage and mechanical rotational frequencies. These

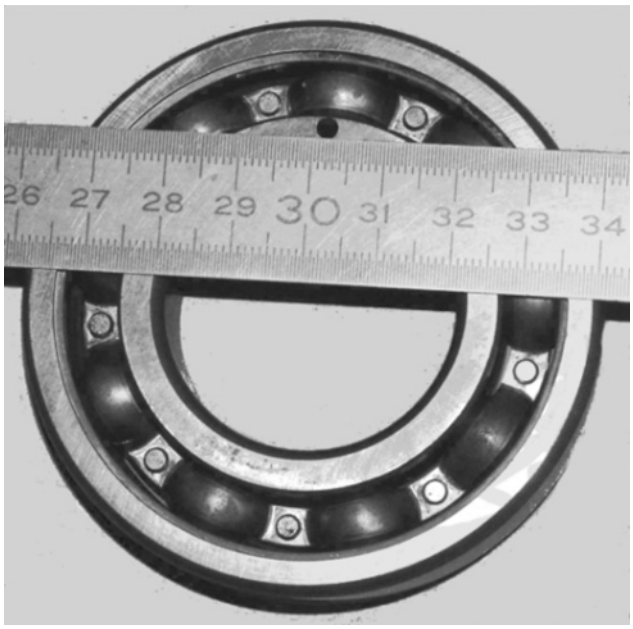

Figure 1 *Photograph of 6208-type bearing with artificial inner race fault*

characteristic frequencies can be expressed using (1) [11].

$$\begin{aligned} f_{\text{orf}} &= \frac{f_{\text{r}}}{2} N_{\text{b}} \left(1 - \frac{D_{\text{b}} \cos\theta}{D_{\text{p}}}\right) \\ f_{\text{irf}} &= \frac{f_{\text{r}}}{2} N_{\text{b}} \left(1 + \frac{D_{\text{b}} \cos\theta}{D_{\text{p}}}\right) \\ f_{\text{c}} &= \frac{f_{\text{r}}}{2} \left(1 - \frac{D_{\text{b}} \cos\theta}{D_{\text{p}}}\right) \end{aligned} \quad (1)$$

where:

- f_{orf} is the outer race fault frequency;
- f_{irf} is the inner race fault frequency;
- f_{c} is the cage frequency;
- f_{r} is the mechanical rotational frequency;
- N_{b} is the number of balls;
- D_{b} is the ball diameter;
- D_{p} is the pitch diameter;
- θ is the contact angle.

2.2 Bearing effects on vibration signals

For localised defects on one of the elements of the bearing, frequencies previously given in (1) appear in the vibration spectrum. Moreover, the outer ring natural frequencies will

also be excited and modulated with the characteristic frequencies [10–12]. Consequently, the knowledge of natural frequencies of the outer ring of the considered bearing is of strong interest for vibration analysis. These natural frequencies can be obtained by measurements, finite element modal analysis or approximate formulas where the outer ring is considered as a cylinder. The formula (2) given in [13] allows to calculate the natural modes of low order for a cylinder with a good confidence rate.

$$f_n = \frac{1}{2\pi}\frac{n(n^2-1)}{\sqrt{n^2+1}}\sqrt{\frac{Elb^3}{12\mu R^4}} \tag{2}$$

where:

- n is the mode order;
- E is the Young's modulus of elasticity;
- μ is the mass per unit length;
- R is the mean radius of the ring;
- l is the width of the ring;
- b is the thickness of the ring;

Considering the physical and geometrical parameters of our 6208-type bearing, the approximate frequencies of the natural modes of the bearing are given in Table 1. An example of the vibration spectrum from an accelerometer positioned near the housing of a 6208-type bearing is given in Fig. 2. It can be noticed that the frequency values given by (2) allow to have a good approximation of natural mode frequencies. Moreover, considering the parameters of the bearing, natural modes have high frequencies. It implies that the spectral study of vibrations considering the mode frequencies requires a high frequency acquisition system.

2.3 Scalar indicators for the detection of bearing faults

Many wear processes can lead to bearing failure, including mechanical damage, lubricant deficiency and corrosion [11]. Generally, the first step of wear is the appearance of generalised fluting or spalling for instance, leading to numerous pitting points and consequently high-frequency

Table 1 Natural mode frequencies for 6208-type bearing

Mode order	Frequency, Hz
2	2309
3	6531
4	12 522
5	20 251

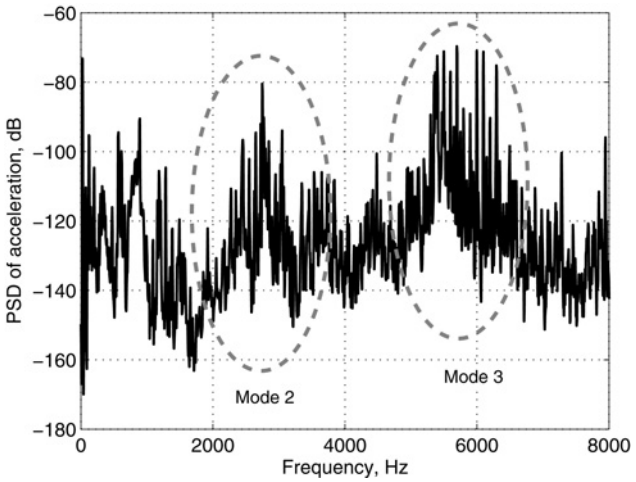

Figure 2 *Power spectral density of vibration of a 6208-type bearing*

vibrations that can excite natural modes. Thus, the peak amplitude of the vibration signal increases. The last step of bearing wear often lies in the appearance of severe indentation, considered as localised defects leading to harmonics on the vibration spectrum at combination of characteristic fault frequencies related to the defect location. Thus, the RMS value of the vibration signal increases.

For a discrete signal x of length N and mean $\bar{x}$, three major scalar indicators are thus defined: the Crest factor (3), the K factor (4) and the Kurtosis (5) [14]

$$\text{Crest} = \frac{\max(|x|)}{\sqrt{(1/N)\sum_{i=1}^{N} x_i^2}} \tag{3}$$

$$K = \max(|x|)\sqrt{\frac{1}{N}\sum_{i=1}^{N} x_i^2} \tag{4}$$

$$\text{kurt} = \frac{(1/N)\sum_{i=1}^{N}(x_i-\bar{x})^4}{\left[(1/N)\sum_{i=1}^{N}(x_i-\bar{x})^2\right]^2} \tag{5}$$

The evolution of the Crest factor indicates the presence of a bearing fault. As a contrary, K factor and kurtosis have to be compared to determined thresholds to detect the presence of a fault. However, these indicators have to be applied on signals with a high sampling frequency to take the natural modes into account.

2.4 Advanced signal processing methods for the detection of bearing faults

Various signal processing methods are used to detect bearing faults on vibration signals. Three major techniques are often presented. The analytic signal resulting from the vibration signal can be computed using the Hilbert transform [15, 16]. The spectrum of the corresponding complex envelope or intrinsic mode functions (IMF) resulting from the

complex envelope allows to detect amplitude modulations at characteristic fault frequencies. However, considering that the Hilbert transform is obtained through the Fourier transform (FT), the Hilbert frequency filtering and the inverse FT, this technique induces a high computation complexity. In order to detect the appearance of modulations or multiples of harmonics at characteristic fault frequencies in vibration spectrum, the cepstrum can be used [17]. This method lies in the computation of twice the FT of the vibration signal, leading to the detection of periodical phenomena into the spectrum. However, this method also induces a high computation complexity. The third detection scheme is the computation of the wavelet or wavelet packet transform [18–20]. The difficulty lies in the choice of the appropriated wavelet, regarding the quality of results and the computation complexity depending on the wavelet filter length K and the analysis level J. Finally, although advanced signal processing techniques are efficient, the resulting computation complexities of previous signal processing methods are given in Table 2 and can be considered as too high to use them in low cost industrial applications.

2.5 Vibration spectral energy detector

These observations concerning scalar indicators and advanced signal processing methods lead us to define a mechanical detector based on spectral energy extraction in vibration spectrum. Consequently, the computation of the detector is only based on the acquisition and the achieving of the FT of the vibration signal. The related computation complexity is recalled in Table 2. The fault detector is defined by extracting energies on frequency ranges related to the frequency components at multiples of f_{def}, where f_{def} is either the inner or the outer race theoretical characteristic frequency. Moreover, the frequency ranges are extended to include modulations linked to the mechanical speed and cage frequencies. The chosen frequency ranges are given in (6). The proposed indicator uses the relative error of energy in the specified frequency ranges between a faulty and healthy reference vibration spectrum. A cumulative sum is then applied on the energy differences extracted from the frequency ranges. Finally, cumulative sums related to outer and inner race frequency ranges are added. The detector value is then defined as the last value of the cumulative sum.

$$\begin{matrix}[nf_{\text{def}} - f_c;\ nf_{\text{def}} + f_c] \\ [nf_{\text{def}} - f_r - f_c;\ nf_{\text{def}} - f_r + f_c] \\ [nf_{\text{def}} + f_r - f_c;\ nf_{\text{def}} + f_r + f_c]\end{matrix} \quad (6)$$

where $n \in [1; 3]$.

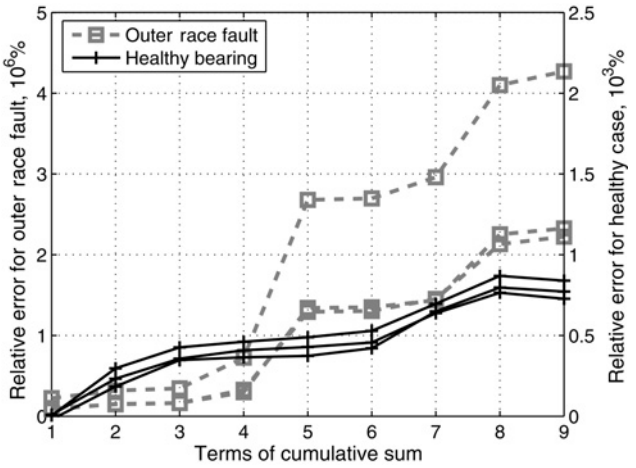

Figure 3 *Mechanical indicator for outer race fault*

As an example of the detector results, Fig. 3 presents this indicator for the detection of localised outer race fault with a supply frequency $f_s = 50$ Hz. Notice that Fig. 3 is double scaled with a factor of 1000 between the two vertical axis. The distinction between healthy and faulty cases can thus be clearly done. This approach certifies that bearing fault detection is possible using the energy in the spectrum of vibration signal. As numerous harmonics due to inner race defect exist in frequency ranges corresponding to outer race fault and reciprocally, setting $f_{\text{def}} = f_{\text{orf}}$ or $f_{\text{def}} = f_{\text{irf}}$ does not guarantee the distinction between inner and outer race faults. Thus, this indicator is built to detect bearing faults whatever these locations on the bearing, by considering outer and inner race fault characteristic frequencies appearance in vibration spectrum.

Comparing to scalar indicators, this indicator needs a low sampling frequency of vibration signals. As a matter of fact, the frequency ranges used in the detection scheme do not exceed 500 Hz, thus the sampling frequency can be limited to 1 kHz, comparing to scalar indicators taking into account the natural modes of the outer ring that need a sampling frequency often higher than 10 kHz.

3 Mechanical effects in case of bearing fault

Before studying the detection of bearing faults on stator currents of the asynchronous machine, it has to be demonstrated that bearing defects induce effects on mechanical quantities. Except vibration appearance, two major effects of bearing faults on mechanical quantities

Table 2 Computation complexity of vibration signal processing methods for the detection of bearing faults

IMF of Hilbert transform	Cepstrum	Wavelet transform	Wavelet packet transform	Spectral energy detector
3 $N \log_2(N)$	2 $N \log_2(N)$	$4KN$	JN (2K 1)	$N \log_2(N)$
4.5×10^6	3×10^6	5.12×10^6	12.16×10^6	1.5×10^6

Example with N 128 000, K 10, J 5

have to be studied. Firstly, a radial eccentricity can be induced by the hole on raceways [7]; then, load torque oscillations can be considered [8].

3.1 Eccentricity due to artificial bearing faults

Artificial bearing faults, considered as severe damaged bearings, may produce a radial displacement of balls when rolling through the hole. According to the geometrical parameters of the 6208-type bearing and the fault dimensions, the radial displacement of a ball ϵ is expressed as (7).

$$\epsilon = R_B\left(1-\sqrt{1-\frac{R_b^2}{R_B^2}}\right) \tag{7}$$

where:

- $R_B \simeq 6.3$ mm is the ball radius;
- $R_b \simeq 1.05$ mm is the apparent half-width of the hole on the surface of the raceway.

Then, the radial displacement of a ball due to the defect is about 90 μm. It has to be noticed that the other balls are not affected by the defect.

In normal conditions, when no balls are affected by the defect, the radial load applied on the bearing, by the weight of the shaft for instance, is distributed on each ball in the load zone of the bearing. When a ball in the load zone is affected by the defect, it does not support any load. Consequently, other balls in the load zone are subjected to an over-load, inducing an indentation of these balls in the raceways depending on the hardness of materials. In this case, according to simulations, the radial displacement of the rotor is about 0.3 μm.

Considering the average airgap length of the machine, namely 800 μm, the relative eccentricity induced by the bearing defects equals 0.0375%. According to the literature, using stator current monitoring, a clear detection of at least 20% of dynamic eccentricity is ensured [21]. Consequently, the eccentricity induced by bearing defects is considered as negligible and non-detectable on stator currents.

3.2 Load torque oscillations due to bearing faults

When a ball rolls through a defect, an impact occurs that induces vibrations and a resistance to the rotation of the bearing and thus a torque disturbance. The experimental spectrum of load torque demonstrates the presence of harmonics at frequencies related to bearing faults. Here, the supply frequency is chosen equal to the nominal one namely 50 Hz. Thus, the mechanical speed equals to about half the supply frequency due to the number of pole pairs (p 2) and the slip of the machine $f_r \simeq f_s/p = 25$ Hz. The outer race fault frequency is around 89 Hz and the inner race frequency is about 136 Hz. Hence, as an example, Fig. 4 shows a part of the mechanical load torque spectra around twice the characteristic fault frequency for inner race fault compared to the healthy case. As for vibration analysis, the load torque oscillation frequencies are combinations of characteristic frequencies of the bearing and rotational frequency. All theoretical combinations do not appear in load torque spectrum and the frequency content cannot be theoretically predicted.

Moreover, for many industrial applications, the implementation of a torque sensor may be a too expensive spending. Consequently, a detector based on load torque spectral analysis has not been yet investigated.

4 Stator current model in case of bearing faults

4.1 Stator current model with load torque oscillations

Previous studies on mechanical failures in induction motors have shown that load torque oscillations induce phase modulations (PM) on stator current [8, 22, 23]. Considering that load torque oscillations are composed of a sum of n harmonics of frequencies f_n and amplitudes Γ_n, the load torque on the shaft of the machine can be expressed using (8). The average load torque is equal to the electromagnetic motor torque that is considered as a constant Γ_0.

$$\Gamma_{\text{load}}(t) = \Gamma_0 + \sum_n \Gamma_n \cos(2\pi f_n t) \tag{8}$$

In case of slight load torque oscillations, the FT of the stator current expression can be approximated by a phase modulated

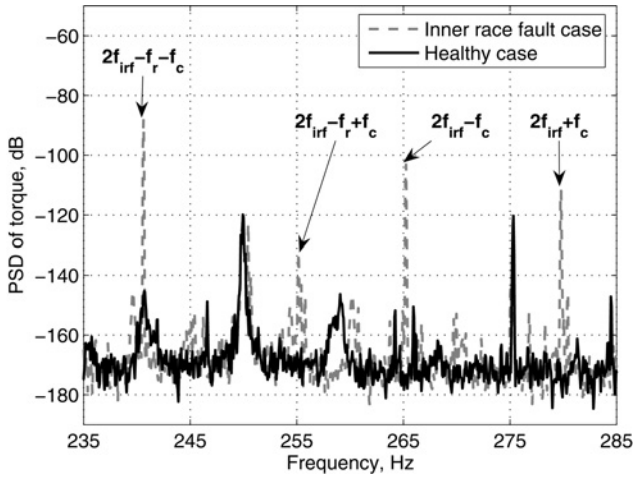

Figure 4 *Spectrum of mechanical load torque – comparison between healthy and inner race fault cases*

signal (9) along the frequency ν [22]. In (9), I_s is the amplitude of stator current, I_r is the amplitude of rotor current and p is the number of pole pairs of the asynchronous machine. Moreover, one can notice that in case of faulty bearings, the frequencies of load torque oscillations f_n may equal any combination of characteristic fault frequencies underlined by the load torque spectrum.

$$|FT\{i(t)\}| = (I_s + I_r)\delta(\nu - f_s) + I_r \sum_n \frac{\beta_n}{2}\delta(\nu - (f_s \pm f_n)) \quad (9)$$

where:

$$\beta_n = f(\Gamma_n, f_n) \quad (10)$$

In (10), f is an unknown function that has to be characterised.

4.2 Amplitude variation law of sideband components

The knowledge of the amplitude variation of stator current sideband components related to the fault frequency, is of strong interest for the detection of bearing faults. Thus, the stator current sideband amplitudes at $f_s \pm f_n$ are studied regarding the load torque oscillation frequency. The corresponding function $\beta_n(f_n, f_s)/\Gamma_n$ is then studied regarding f_n and f_s.

Consider the general model of an electrical drive. On the one hand, the model is composed of a mechanical subsystem with load and electromagnetic torques as entries and rotational speed as output. On the other hand, the model is composed of an electrical subsystem with rotational speed and stator voltages as entries, electromagnetic torque as output and stator currents as intermediate variables. It is understandable that both the mechanical and electrical models must be taken into account to establish the link between stator currents and load torque. In a general approach, mechanical and electrical transfer functions are at least of first order. Thus, even if mechanical and electrical transfer functions are non-resonant, the corresponding transfer function resulting from their association may present a resonant behaviour with an order greater or equal to 2. The existence of this resonance is related to electrical and mechanical parameters values of the models.

Due to the product of currents and fluxes to obtain the electromechanical torque, a complete analytical approach cannot be performed to determine $\beta_n(f_n, f_s)/\Gamma_n$. To obtain suitable information concerning the variation law of sideband components on the stator current with regard to the load torque oscillation frequency, a simulation approach is proposed. Firstly, a state model of the motor is associated with a first-order mechanical model composed of an inertia plus a friction. An oscillating load torque with variable frequency f_n is added to the mean load torque and amplitude of sideband components at $f_s \pm f_n$ in the stator current are extracted from its spectrum. Using electrical and mechanical parameters of the set-up, the simulation demonstrates that a natural resonance exists in the drive. Moreover, the resonance characteristics, in terms of gain and frequency, also depend on the motor operating point. Fig. 5 underlines this point by depicting the gain diagram $20\log_{10}(\beta_n(f_n, f_s)/\Gamma_n)$ along the load torque oscillation frequency f_n and the supply frequency of the induction machine f_s. The level of grey depicts the gain value. In a second time, a more complete mechanical model is introduced.

The physical set-up is composed of the asynchronous motor coupled to a DC motor used as a load. The mechanical system is composed of inertias of the motor and the load, frictions and and a coupling stiffness. Parameters of the mechanical transfer function come from the manufacturer datasheets and a mechanical resonance around 20 Hz can be pointed out. The whole drive model, including the previous mechanical model, is simulated and compared to measurements achieved on the experimental set-up. The DC machine is connected to a resistor through a DC/DC converter that controls the DC motor armature current. In order to obtain the experimental gain diagram $\beta_n(f_n, f_s)/\Gamma_n$, the reference current of the DC/DC converter is composed of an oscillating component plus an offset in order to induce load torque oscillations around a mean load torque value. Fig. 6 depicts the experimental gain diagram for several supply frequencies (f_s 50 Hz, f_s 13.3 Hz and f_s 6.7 Hz) and the simulated one for f_s 50 Hz. The main observation lies in the existence of an experimental and simulated resonance point around $f_{res} \simeq 20$ Hz. It can be noticed that even if the resonance amplitude varies, the resonance frequency is almost constant whatever the considered supply frequency. This observation is confirmed by simulation. Comparing to the simulation results obtained with a first-order mechanical

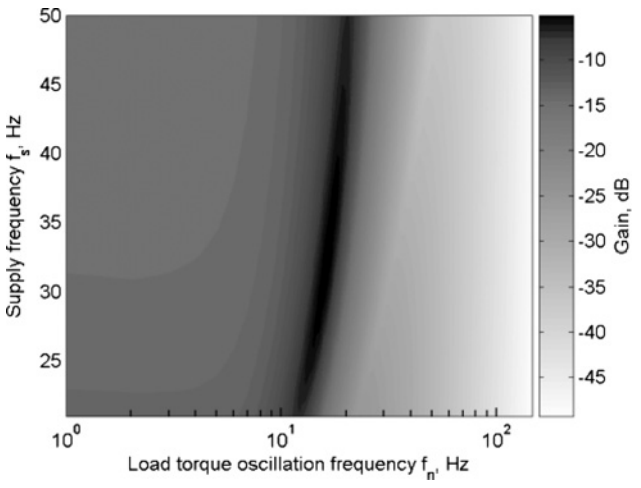

Figure 5 *Simulated 3D gain diagram 20 log$_{10}$ [β_n/Γ_n] with a non-resonant mechanical transfer function for 20 Hz $\leq f_s \leq$ 50 Hz*

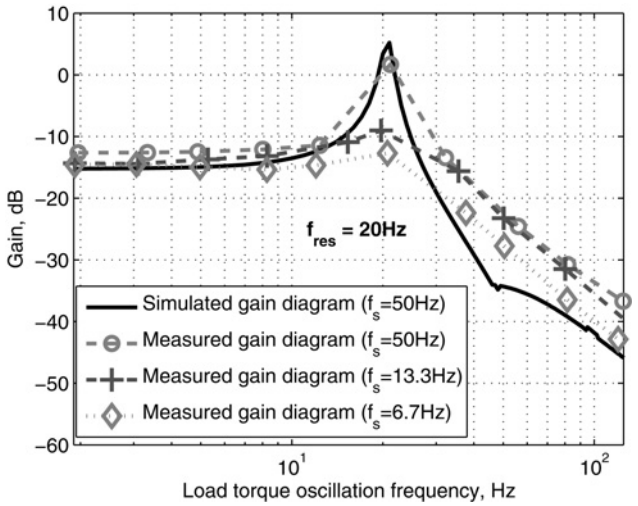

Figure 6 *Experimental and simulated gain diagrams of sideband components on stator current for several supply frequencies*

model (Fig. 5), it can be said that accurately modelling the mechanical part of the drive allows to be more realistic in order to predict the whole frequency behaviour of the set-up. According to the frequency response of the electromechanical test bench and assuming that a bearing defect creates slight load torque oscillations at one of the characteristic frequencies determined in (1), the resonance point may be used as a natural amplifier to obtain amplified PM harmonics on stator current. It has to be noticed that gain diagrams depicted in Fig. 6 are deeply associated with the considered test bench. However, using this simulation method, accurately modelling the mechanical system and identifying electrical parameters of a machine, the gain diagram of any induction drive may be established.

5 Stator current spectral detector for bearing faults

As shown in Section 3.2, bearing defects induce load torque oscillations and consequently, PM on stator current. However, the amplitude of these PM is quite slight and could be buried in noise. Some techniques are used to reduce the stator current signal-to-noise ratio (SNR). The fast Fourier transform (FFT) of two stator currents is performed and resulting spectrums from the two phases are multiplied to correlate signatures [24]. This method allows improving the efficiency of fault harmonics detection.

5.1 Definition of spectral indicator S

Similarly to the vibration analysis and according to the stator current model (9), the detector S is defined by extracting energies on frequency ranges corresponding to the sideband components at $f_s \pm nf_{def}$ where f_{def} is either the inner or the outer theoretical mechanical fault frequency. Moreover, as for mechanical torque analysis, the frequency content of stator current in case of bearing faults cannot be theoretically evaluated. Thus, as a contrary to other studies that generally focus on the detection of specific harmonics is stator current spectra, such as in [9], the proposed indicator takes into account the probabilistic nature of stator current harmonics due to bearing defects. This allows to consider the possible appearance of numerous harmonics on stator currents related to bearing faults by analysing a global energy increase in frequency ranges. Thus, the frequency ranges are extended to include modulations linked to the cage and mechanical rotational frequencies underlined by the vibration and the mechanical load torque spectral analysis (see Fig. 4). Chosen frequency ranges are given in (11).

$$\begin{aligned} &|f_s \pm [nf_{def} - f_c;\ nf_{def} + f_c]| \\ &|f_s \pm [nf_{def} - f_r - f_c;\ nf_{def} - f_r + f_c]| \\ &|f_s \pm [nf_{def} + f_r - f_c;\ nf_{def} + f_r + f_c]| \end{aligned} \tag{11}$$

where $n \in [1; 5]$.

Notice that in case of current spectral analysis, the mechanical rotational frequency is estimated via slot harmonics on stator current [25]. Moreover, bearings manufacturer often provide characteristic frequencies for a given rotational frequency. According to (1), using the proportionality between rotational speed and characteristic frequencies, these ones are estimated for the computed rotational speed. For the induction machine under test, the maximum slot harmonic frequency is 750 Hz for the maximum supply frequency. As a comparison, the maximum frequency analysed in the bearing fault detection scheme is $f_s + 5f_i rf + f_r + f_c \simeq 765$ Hz. Consequently, the sampling frequency can be limited to 2 kHz and the detection of slot harmonic does not change the sampling frequency of stator current. In each frequency range, the spectral energy is estimated and normalised by the maximum value in the considered range.

Then, the proposed indicator uses the relative error of energy between the current spectrum in faulty and healthy cases in the specified frequency ranges. Thus, the relative errors of energy extracted from frequency ranges related to outer and inner race fault are added in order to obtain a single energy difference. Finally, a cumulative sum is used to build the indicator. Only the last value of the cumulative sum is considered as the detector value.

5.2 Detection of localised faults using the resonance point

To illustrate the computation of the detector values, a detailed example is given for detector S in case of a localised outer or inner race fault and healthy bearing. A common healthy energy reference is used for the three bearing cases. The figures show cumulative sums corresponding to the computation of detector S. For the detection of localised faults, three experimental conditions are tested, corresponding to three different supply

frequencies. In Fig. 7*a*, the supply frequency f_s is tuned to 13.3 Hz in order to ensure $f_{orf} = f_{res}$. In Fig. 7*b*, the supply frequency f_s is tuned to 6.7 Hz to ensure $f_{irf} = f_{res}$. In Fig. 7*c*, the supply frequency f_s is tuned to 50 Hz, corresponding to the nominal supply frequency of the machine. In this case, $f_{irf} = 136$ Hz and $f_{orf} = 89$ Hz and no characteristic fault frequency equals to the resonance point. The PM signatures are located in the attenuation part of the electromechanical gain diagram (see Fig. 6). Fig. 7*c* underlines that distinction between healthy and faulty cases is not possible with this detector when the sideband components are strongly attenuated. It emphasises the importance of properly tune the supply frequency to ensure the detection of a possible bearing fault.

Moreover, as expected, properly tuning the frequency supply leads to focus on inner or outer race fault. When f_s is set to guarantee $f_{orf} = f_{res}$, the effects on stator currents of load torque oscillations due to the outer race localised fault are amplified by the resonance point and the detection of the outer race fault is ensured. Reciprocally, using the similar amplification effects, the detection of the inner race fault is ensured when f_s is set to guarantee $f_{irf} = f_{res}$.

5.3 Detection of naturally damaged bearing using the resonance point

The detector S is applied on stator currents to detect faults on naturally damaged bearings that was rejected by a vibration analysis performed in the after-sales service of a motor manufacturer. The fault types or locations are unknown. According to the detection scheme and the exploitation of the resonance point, the detector S is computed in healthy and faulty cases for the two emphasised operating points ($f_s = 6.7$ Hz and $f_s = 13.3$ Hz). In case of the detection of possible inner race fault ($f_s = 6.7$ Hz), the faulty detector is clearly higher than the healthy one which is close to zero as it can be seen in Fig. 8. This result proves that inner race faults affect the damaged bearing. A vibration spectrum is also performed to reinforce the assumption of the presence

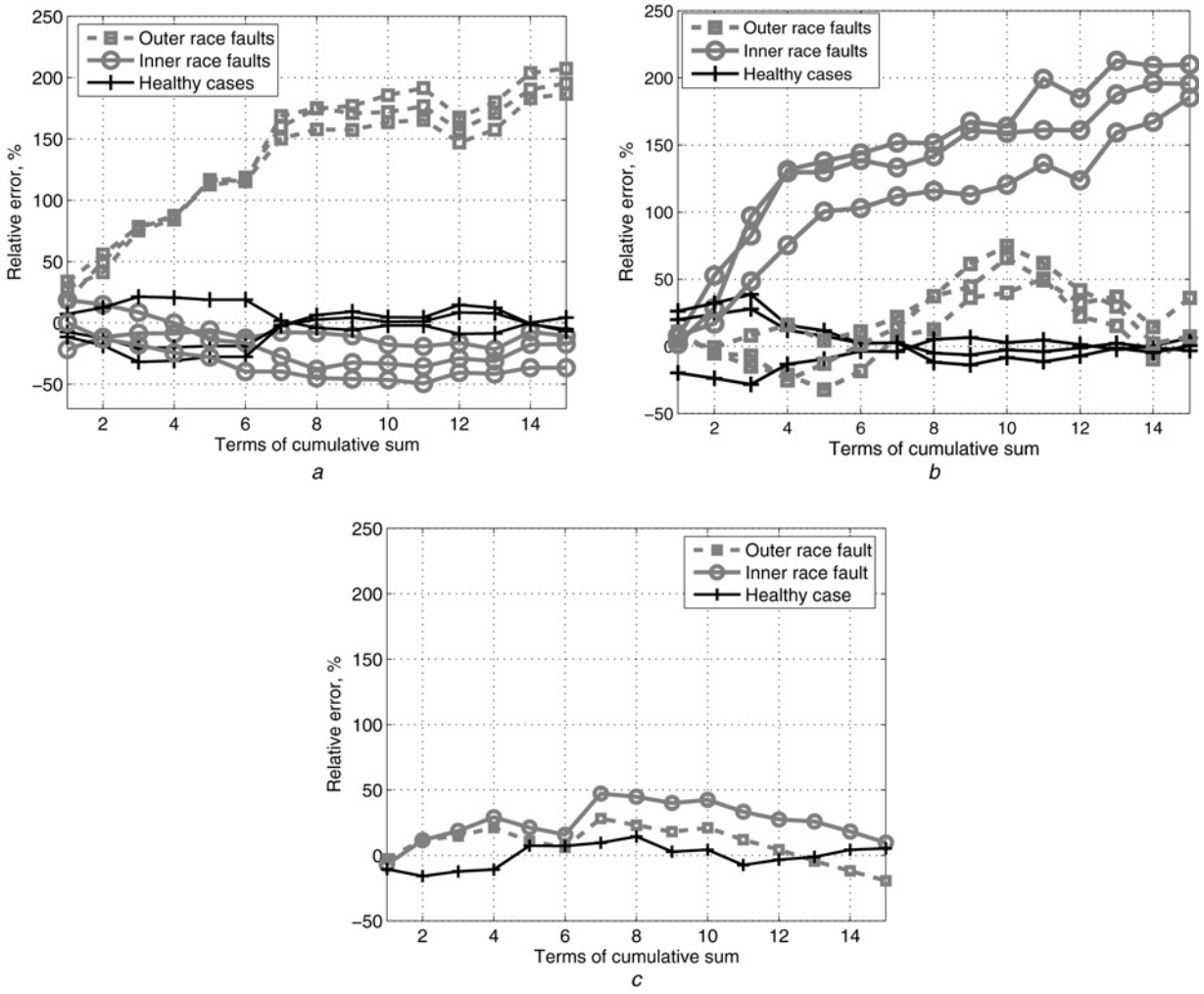

Figure 7 *Cumulative sums of relative error in %*

a $f_{orf} \simeq f_{res}$
b $f_{irf} \simeq f_{res}$
c $f_s = 50$ Hz

of inner race defects. Several fault harmonics related to inner race characteristic frequency appear in the vibration spectrum according to Table 3.

5.4 Discussions on the proposed indicator

The proposed indicator is restricted by the electromechanical behaviour of the experimental set-up. This resonance allows to amplify the effects of load torque oscillations on stator current and consequently improve the detection efficiency. Consequently, the characteristic fault frequencies f_{orf} or f_{irf}, depending on the rotational frequency and thus on the supply frequency of the induction machine, have to be close to the resonance frequency. This is achieved by tuning the supply frequency to ensure that one of the characteristic frequencies equals the resonance point. Moreover, it means that the detection of bearing defects by the proposed indicator becomes underachiever for any other supply frequency, especially for the nominal supply frequency where the characteristic fault harmonics are high frequency, filtered by the electromechanical gain diagram depicted in Fig. 6. Consequently, the detection of bearing faults is necessarily determined by the electromechanical behaviour of the system and the ability of tuning the supply frequency of the induction motor to take into account the possible resonance points.

It can be noticed that this indicator is less sensitive than the one based on vibration signals. However, the interest of this method lies especially in the cost of instrumentation. Vibration analysis needs well positioned accelerometers near each bearing that has to be monitored. This instrumentation is often incompatible with low cost drives such as induction drives. As a comparison, the monitoring based on stator current analysis only needs current sensors such as Hall effect sensor or current transformer such as Rogowski coil sensor [26]. These sensors are often already used for control and protection purposes. Moreover, as for the vibration spectral detector, the stator current indicator needs a low sampling frequency especially for low supply frequencies.

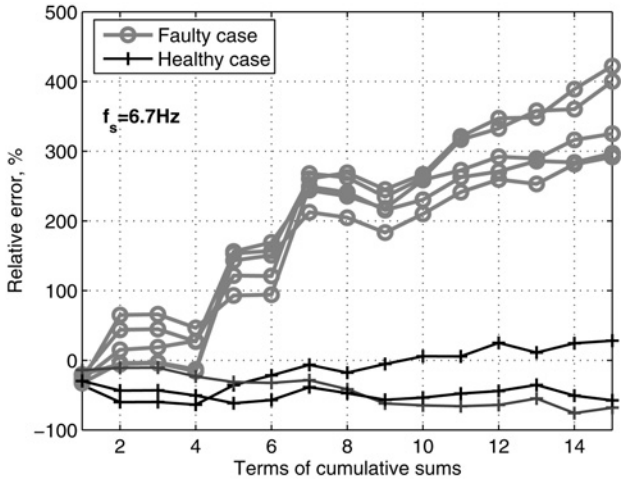

Figure 8 *Cumulative sums of relative error in % for the detection of naturally damaged bearing*

Table 3 Example of fault harmonics in vibration spectrum of a naturally damaged bearing for f_r 25 Hz

Harmonic frequency	Energy variation, dB
$f_{irf} + f_r - \frac{f_c}{2}$	+21
$2f_{irf} - \frac{f_c}{2}$	+26.5
$2f_{irf}$	+31
$3f_{irf} + f_r$ f_c	+27
$3f_{irf} + f_r$	+18.8

5.5 Suggestions for the choice of a detection method

The choice of a detector depends on the monitored system. When the supply frequency is variable and can be set to a low value, depending on the electromechanical behaviour of the system, the stator current spectral indicator can be used to detect faults due to wear on bearings. This method is particularly appropriated for industrial systems where a diagnosis procedure can be operated periodically, for instance before starts of the mission of the machine.

However, when the machine is running at a unique speed that does not allow to use the resonance point, the vibration analysis has to be used. In this case, the automatic detector can be preferred to scalar indicators or advanced signal processing methods due to the high computation performances required. In order to follow the wear process of bearings, the scalar indicators are well appropriated but the acquisition system has to be of high frequency sampled.

6 Conclusions

In this paper, some methods for the detection of bearing faults in induction motors using vibration and stator current monitoring have been presented. On artificially damaged bearings, a vibration spectrum analysis has been proposed to detect and diagnose the faults. This method has been compared to classical techniques such as scalar indicators and advanced signal processing methods. Mechanical considerations have shown that bearing defects induce preferentially load torque oscillations comparing to eccentricity. Thus, the effects of load torque oscillations on stator current have been recalled. The amplitude variation law of the stator current components has been determined by experimental measurements and simulation results. The resonance point has been used to amplify slight load torque oscillations and to allow detecting preferentially inner or outer race fault. An automatic detector based on stator current spectral analysis has been presented and validated on localised faults and naturally damaged bearing.

Comparison between vibration and stator current indicators has been presented. Restrictions of the detector concerning its

definition and the consideration of the electromechanical behaviour of the test bench have been discussed. This has led to indications concerning the choice of detection methods depending on the considered system. Compared to vibration analysis, the stator current detector needs less expensive instrumentation. However, the vibration indicator is usable in several applications. To extend the application of fault detection, condition monitoring on variable speed drives could be studied by using time-frequency or time scale analysis to detect bearing faults at the start-up of the machine. Moreover, other faulty conditions such as lubricant contamination or grease wear could be investigated on stator current along the lifetime of the bearing. Finally, other mechanical quantities such as mechanical speed or torque can be studied by measurements or estimation.

7 References

[1] TAVNER P.J., RAN L., PENMAN J., SEDDING H.: 'Condition monitoring of rotating machines' (The Institution of Engineering and Technology, London, 2008, 2nd edn.)

[2] RAISON B., ROSTAING G., BUTSCHER O., MARONI C.S.: 'Investigations of algorithms for bearing fault detection in induction drives'. Proc. IEEE Conf. Industrial Electronics Society, November 2002, vol. 2, pp. 1696–1701

[3] MCINERNY S.A., DAI Y.: 'Basic vibration signal processing for bearing fault detection', *IEEE Trans. Educ.*, 2003, **46**, (1), pp. 149–156

[4] NANDI S., TOLIYAT H.A.: 'Condition monitoring and fault diagnosis of electrical machines – a review', *IEEE Trans. Energy Convers.*, 2005, **20**, (4), pp. 719–729

[5] STACK J.R., HABETLER T.G., HARLEY R.G.: 'Fault classification and fault signature production for rolling element bearings in electric machines', *IEEE Trans. Ind. Appl.*, 2004, **40**, (3), pp. 735–739

[6] LI W.D., MECHEFSKE C.K.: 'Detection of induction motor faults: a comparison of stator current, vibration and acoustic methods', *J. Vib. Control*, 2006, **12**, (2), pp. 165–188

[7] SCHOEN R.R., HABETLER T.G., KAMRAN F., BARTHELD R.G.: 'Motor bearing damage detection using stator current monitoring', *IEEE Trans. Ind. Appl.*, 1995, **31**, (6), pp. 1274–1279

[8] BLODT M., GRANJON P., RAISON B., ROSTAING G.: 'Models for bearing damage detection in induction motors using stator current monitoring'. Proc. IEEE Int. Symp. on Industrial Electronics, May 2004, vol. 1, pp. 383–388

[9] JUNG J.H., LEE J.J., KWON B.H.: 'Online diagnosis of induction motors using MCSA', *IEEE Trans. Ind. Electron.*, 2006, **53**, (6), pp. 1842–1852

[10] GUYER R.A.: 'Rolling bearings handbook and troubleshooting guide' (Chilton Book Company, Radnor, Pennsylvania, 1996)

[11] HARRIS T.A.: 'Rolling bearing analysis' (Wiley, New York, 1991, 3rd edn.)

[12] OHTA H., KOBAYASHI K.: 'Vibrations of hybrid ceramic ball bearings', *J. Sound Vib.*, 1996, **192**, pp. 481–493

[13] DEN HARTOG J.P.: 'Mechanical vibrations' (Dover Books on Engineering, Dover Publications, New York, 1985), pp. 165–167

[14] BOLAERS F., COUSINARD O., MARCONNET P., RASOLOFONDRAIBE L.: 'Advanced detection of rolling bearing spalling from de-noising vibratory signals', *Control Eng. Pract.*, 2004, **12**, pp. 181–190

[15] FLANDRIN P.: 'Time-frequency/time-scale analysis' (Academic Press, San Diego, 1999)

[16] RAI V.K., MOHANTY A.R.: 'Bearing fault diagnosis using FFT of intrinsic mode functions in Hilbert Huang transform', *J. Mech. Syst. Signal Process.*, 2007, **21**, (6), pp. 2607–2615

[17] BOGER B.P., HEALY M.J.R., TUKEY J.W.: 'The quefrency analysis of time series for echoes: cepstrum, pseudo-autocovariance, cross-cepstrum and saphe cracking'. Proc. Symp. Time Series Analysis, 1963, pp. 209–243

[18] MALLAT S.: 'A wavelet tour of signal processing' (Academic Press, San Diego, 1998)

[19] EREN L., DEVANEY M.J.: 'Bearing damage detection via wavelet packet decomposition of the stator current', *IEEE Trans. Instrum. Meas.*, 2004, **53**, (2), pp. 431–436

[20] RUBINI R., MENEGHETTI U.: 'Application of the envelope and wavelet transform analyses for the diagnosis of incipient faults in ball bearings', *J. Mech. Syst. Signal Process.*, 2001, **15**, (2), pp. 287–302

[21] DORRELL D.G., THOMSON W.T., ROACH S.: 'Analysis of airgap flux, current, and vibration signals as a function of the combination of static and dynamic airgap eccentricity in 3-phase induction motors', *IEEE Trans. Ind. Appl.*, 1997, **33**, (1), pp. 24–34

[22] BLODT M., CHABERT M., REGNIER J., FAUCHER J.: 'Mechanical load fault detection in induction motors by stator current time-frequency analysis', *IEEE Trans. Ind. Appl.*, 2006, **42**, (6), pp. 1454–1463

[23] SCHOEN R.R., HABETLER T.G.: 'Effects of time-varying loads on rotor fault detection in induction machines', *IEEE Trans. Ind. Appl.*, 1995, **31**, (4), pp. 900–906

[24] TRAJIN B., REGNIER J., FAUCHER J.: 'Bearing fault indicator in induction machine using stator current spectral analysis'. Proc. Power Electronics Machine and Drives Conf., April 2008, pp. 592–596

[25] NANDI S., AHMED S., TOLIYAT H.A.: 'Detection of rotor slot and other eccentricity related harmonics in a three phase induction motor with different rotor cages', *IEEE Trans. Energy Conver.*, 2001, **16**, (3), pp. 253–260

[26] PONCELAS O., ROSERO J.A., CUSIDO J., ORTEGA J.A., ROMERAL L.: 'Design and application of Rogowski coil current sensor without integrator for fault detection in induction motors'. Proc. IEEE Int. Symp. on Industrial Electronics, July 2008, pp. 558–563